Bioorganic Chemistry 58 (2015) 53–64

Contents lists available at ScienceDirect

Bioorganic Chemistry

journal homepage: www.elsevier.com/locate/bioorg

Quinoxalines as potent selective CRFRs ligands for monitoring and brain diagnostic

Bojidarka Ivanova *, Michael Spiteller

Lehrstuhl für Analytische Chemie, Institut für Umweltforschung, Fakultät für Chemie, Universität Dortmund, Otto-Hahn-Straße 6, 44227 Dortmund, Nordrhein-Westfalen, Germany

ARTICLE INFO

Article history:
Received 22 July 2014
Available online 20 November 2014

Keywords:
Quinoxalines
CRFRs
Brain diagnostic

ABSTRACT

The paper highlighted quinoxalines as potent ligands to corticotropin-releasing factor receptor types 1 and 2. The content includes design and structure–activity relationship of **50** model substances to $CRFR_1$, $CRFR_{2\alpha}$ and $CRF_{2\beta}$, respectively. It is important to bear in mind, that our concept has based on challenging research task, designing for selective CRFRs ligands. Because,: (i) These macromolecules can bond more than one ligand, thus causing for a distinct physiological response; (ii) CRFRs also participate readily in protein–protein interactions; (iii) CRFRs have two step activation mechanism and; (iv) $CRFR_1$ has low selectivity. In spite of, numerous research efforts, which have been devoted to the isolation of series peptidic and non-peptidic CRFRs agonists, the poor penetration across blood–brain barrier restricts, their wide application in the clinical practice. Furthermore, the biological role of $CRFR_2$ is not yet fully understood. For that reason, the studies of the structure–activity relationship have significant impact in the field. The great advantages of quinoxalines as prospective ligands are based on their: (a) One-step synthetic road, using mild experimental conditions and, allowing to involve various functional groups in the molecular scaffold as well as good-to-excellent yields, employing Fischer and Hinsberg methods; (b) High selectivity to CRFRs sub-types and; (c) Tunable fluorescence emission within the frame of a large scale of the electromagnetic spectrum ∈ 500–700 nm.

1. Introduction

Corticotropin realizing factor is a key element, involved in stress response modulation [1–13]. It biological activity has been associated with mental disorders or diseases such as depression, anxiety, Alzheimer's disease and drug abuse. For that reason, selective CRF antagonists may be implicated in treatment of such disorders [1–13]. The main role of CRF has been associated with activity of hypothalamic–pituitary–adrenal axis in pituitary adrenocorticotropin hormone synthesis. But, the hyperactivity of HPA is supported by diagnosis of depression and anxiety. Furthermore, recent studies have evidenced that HPA is implicated as target for treatment of substance abuse and drug-related behaviours as well as an implementation of CRF antagonists in the treatment of these diseases as well. It has shown that the use of alkyl-(7-substituted-phenyl-7H-pyrrolo[2,3-d]pyrimidin-4-yl)-amines and alkyl-(8-substituted-phenyl-pyrazolo[1,5-a][1,3,5]triazin-4-yl)-amines, which have been implicated in the clinical practice as CRF antagonists, reduces the cocaine self-administration and reinstatement of cocaine and/or opioid-dependent behaviours [1–13]. The largest part of the research efforts have been focused on various CHR ligands, involving peptidic analogous such as, for example, astressin B or non-peptidic small molecular templates, having phenyl-7H-pyrrolo[2,3-d]pyrimidin-4-yl)-amine, phenyl-pyrazolo[1,5-a][1,3,5]triazin-4-yl)-amine or 2,N,N-trialkil-5-alkilsulfanyl-N′-phenyl-pyrimidine-4,6-diamine molecular structure [7,14–18]. The CRF peptide family has involved

Abbreviations: ACHT, adrenocorticotropin; Ant, antalarmin; APCI, atmospheric pressure chemical ionization (mass spectrometric method); CT, charge transfer; CRF, corticotropin realizing factor (equivalent of corticotropin realizing hormone); CRH, corticotropin realizing hormone; $CRFR_1$, corticotropin-releasing factor receptor type 1; $CRFR_2$, corticotropin-releasing factor receptor type 2; CNS, central nervous system; DHA, 2,4-dihydroxy benzoic acid; DHB, 2,5-dihydroxy benzoic acid; DMF, dimethylformamide; EAS, electronic absorption (spectra); ECD, extracellular domain; ESI, electrospray ionization (mass spectrometric method); FF, Force field calculations; Fs, fluorescence spectra (Fs); HPA, hypothalamic–pituitary–adrenal axis; HPLC, high performance liquid chromatography; LODs, concentration limit of detection (analyte); LOQs, concentration limit of quantitation (analyte); MALDI, matrix/assisted laser desorption ionization (mass spectrometric method); MM, molecular mechanics (computational approach); MD, molecular dynamics (computational approach); MS, mass spectrometry; MS/MS, mass spectrometry in a tandem mode of operation; NMR, nuclear magnetic resonance; PE, potential energy; PCM, polarisable continuum method; Ps, phosphorescence; TMD, transmembrane domain.

* Corresponding author. Fax: +49 231 755 4084.
E-mail addresses: B.Ivanova@infu.uni-dortmund.de, B.Ivanova@web.de (B. Ivanova).

http://dx.doi.org/10.1016/j.bioorg.2014.10.008
0045-2068/

an activation of two G-protein coupled receptors, *i.e.* $CRFR_1$ and $CRFR_2$, respectively [1–13]. In particular, the CRF has high affinity towards $CRFR_1$. In spite of, the fact that it bonds $CRFR_2$ effectively [2]. These interactions have been found as important ones to activate the HPA. Therefore, it is of primary interest a molecular design for selective medications for treatment of mental depression, anxiety and substances abuse. The CRF receptors 1 and 2 belong to B-class G-protein coupled receptors, which are organized in two modular domains. The ECD has responsible function to the binding affinity and specificity. While, the second helical bundle domain or the transmembrane domain modular has been involved in the activation of the receptors and the signal coupling [19–22]. Nevertheless, that the structures of full the length receptors are still unknown, more recent structural experiments carried out, showing that ECD allows a theoretical molecular design of new potent ligands, using approaches for the elucidation of the structure–activity relationship [19–22]. A comprehensive comparative analysis between both the class A and B G-protein coupling receptors has shown, that unlike class-A receptors, involving for example dopamine D_3-receptor, the TMD in $CRFR_1$ exhibits V-shape macromolecular architecture with a large molecular cavity. It allows a binding of the neuropeptides of CRF family [19–22]. Superposing of the structures of both receptor classes has shown a striking difference in the ECD. The superposition of their cytoplasmic sides is able to explain, why they have the same effector proteins involved in the signalling processes. Further efforts in the structural studies have resulted in the discovery that CRF receptor 2 has three subtypes, *i.e.* $CRFR_{2\alpha}$, $CRF_{2\beta}$ and $CRF_{2\gamma}$ ones, respectively [3,19–22]. Moreover $CRF_{2\beta}$ is the major ligand recognition domain [8]. The $CRFR_1$ and $CRFR_2$ have similar structure, but they are located in the different places in the brain. So that, the role of the first receptor type has been associated with mediation of the stress, while the biological function of $CRFR_2$ is still not well understood. It has hypothesis, that the biological function includes a modulation of the cardic activity, because of the $CRFR_2$ is disposed on arteriosus in the brain [3]. Nonetheless, that few findings have shown an involvement of the last receptor type in the modulation of the CNS stress response [8]. It has evidences, too, for the mediation of the hypertension through the central $CRFR_1$ receptors [3]. Nevertheless that the participation of the peripheral $CRFR_1$ receptors in such as effect cannot be ruled. The peptide activity has rather been associated with the peripheral receptors, than those ones disposed in the CNS, where the discussed peptidic family has limited accesses. In general, there have evidences, suggesting that $CRHR_1$ has important role for the psychopathology of the modulation of the stress. Given that, the molecular design of selective ligands towards the different corticotropin-releasing factor receptor sub types, and in general, the studies, including the structure–activity relationship are important research task, having significant impact in:

(i) Further understanding of the biological role of the various $CRFR_1$, $CRFR_{2\alpha}$ and $CRF_{2\beta}$ subtypes and the corresponding molecular level biochemical activation mechanisms; (ii) psychopathology of the mental disorders and diseases such as depression, anxiety, Alzheimer's disease and drug abuse; (iii) *in vivo* imaging, monitoring and brain diagnostic approaches and: (iv) molecular design of new selective medications for treatment of such as disorders and diseases, respectively. Furthermore, more recent findings have shown that such derivatives have high affinity as agonists, partial agonists and antagonists to $5\text{-}HT_{3A}$ receptors in central and peripheral nervous systems at sub-micro-molar level [23].

Although, it has significant progress in the molecular design of peptidic and non-peptide CRF antagonists, the drugs-design of novel potent derivatives represents a significant challenge. The class-A ligands, for example, have been used widely, but it has low number of known ligands of class B [21]. The main reasons for such as challenging molecular design, have the following origin: (a) Class B receptors have ability to bind more than one ligand; (b) Different ligands may induce distinct physiological response of the various CRFRs; (c) Receptor macromolecules can participate in numerous protein–protein interactions, in addition to the corresponding ligand–protein and ligand–ligand bonding ones; (d) For this receptor family it has been proposed two step activation mechanism [1–13,19–22]; (e) In general, the $CRFR_1$ has a lower ligand selectivity and; (f) Different affects on the cardic function has been found for CRF. When it has been connected introcerebroventricularly, it induces hypertension. Another important data derive from the studies of the CNS receptors or involving an intravenously access, showing a hypotension affect [1]. The CRF analogue, astressin B, stimulates attenuated ACTH as well. By contrast, antalarmin, which has been described as most promising non-peptidic antagonist having alkyl-(7-substituted-phenyl-7H-pyrrolo[2,3-d]pyrimidin-4-yl)-amines molecular scaffold, exhibits selective function as CRF antagonist with a highlighted affinity to $CRFR_1$ *in vitro*. However, it has self-limited affect *in vivo*. Antalarmin stimulates HPA, too, but at high doses. These, in fact, paradoxical results, have been found their explaining, using the different chemical behaviour and solubility in water of astressin B and **Ant,** thus causing for an application of **Ant** as an emulsion composition, which can result to a poor distribution. But, in parallel, it has available hypothesis that antalarmin can exhibit new activity profile, including blockade of both central and peripheral receptors of 1 type [1]. In spite of, enormous research efforts in the development of peptidic and non-peptidic CRF antagonists, as well as numerous *in vitro* and *in vivo* tests, the clinical use of various of peptidic analogous is limited, due to reason mentioned above, *i.e.* reason (e). In addition, they have poor penetration properties to across blood–brain barrier. Nevertheless, peptide–based therapeutics have gradually expanded, thus causing for further efforts in the their development [24]. The promising data for non-peptidic derivatives of alkyl-(7-substituted-phenyl-7H-pyrrolo[2,3-d]pyrimidin-4-yl)-amine, alkyl-(8-substituted-phenyl-pyrazolo[1,5-a][1,3,5]triazin-4-yl)-amine and/or 2,N,N-trialkil-5-alkilsulfanyl-N′-phenyl-pyrimidine-4,6-diamine type are also encouraged. Nevertheless, that they have known poor solubility, due to a high lipophilicity, which restrict a wide clinical using. These paradoxical and often contradiction discoveries about the biological functions and role of the peptidic and the known non-peptidic CRFRs antagonist; about the still not fully understood biological role of $CRFR_2$ themselves and; accounting for the chemical properties of the known non-peptidic ligands, causes for a search of new ligands for treatment of mental disorders such as major depression, anxiety, Alzheimer's disease and drug abuse; or substances for *in vivo* imaging, monitoring and brain diagnostics, which is no dough an emergent and challenging task in the frontier of the medicinal chemistry. It is important, however, to bear in mind, that from chemical point of view, it is difficult to balance the properties of the new ligands between their, of one site, high selectivity to different CRFRs and, in parallel, ability for penetration of the blood–brain barer; or high selectivity to different CRFRs and suitable optical properties for imaging and brain diagnostics, only localizing the research efforts to the given small number of both peptidic and non-peptidic classes of chemical substances. An effective solution of the scientific problems, highlighted above in (a)–(f), can be found, examining both theoretically and experimentally a large number of chemical classes, which able to differentiate between the important molecular level structural factors, causing for the high selectivity to the CRFRs sub-types; to a high efficiency towards the blood–brain barer penetration and; suitable optical properties allowing imaging and brain diagnostics. For that reason, in this study, we have chosen a strategy to change completely the molecular scaffold of the non-peptidic ligands, introducing a new specific skeleton, which allows: (A) An easy and step-limited synthesis; (B) Substitution of various functional groups, allowing different molecular engineering models of

the binding affinity of the ligands towards the macromolecules and; (C) An easy tuning of the optical properties of the ligands within the frame of a large scale of the electromagnetic spectrum.

So that, we have reported essentially new class of non-peptidic ligands as potential selective $CRFR_2$ agonists, which can find application for the brain diagnostics and monitoring. They could also have application as therapeutics, balancing between a high receptor selectivity and ability to penetrate the blood–brain barer.

Nonetheless, that our past and ongoing studies have been focused mainly on potential medications on the base on naturally occurring molecular templates with large scale of physiological activity, involving in anticancer, antimicrobial and/or antiplasmodial function [25–27], this study have concentrated the attention on synthetic substances, having affinity towards CRFRs.

2. Experimental

2.1. Synthesis

Quinoxalins, depicted in Scheme S1 were synthesized, according Scheme 2 [28–46]. The single-step synthesis of [1,4]-dioxino [2,3,b]pyrazine motif in **1–4**, **9–13** and **46–50** as well as the 12H-5-oxa-6,11,12-triaza-naphthacene one in **5–8** and **15–19** was achieved, using the cyclocondensation in DMF through mixing of equimolar amounts of substituted 2,3-dichloroquinoxaline (4.0 g), preliminary dissolved in 20 mL of heated DMF with solution (or suspension) of corresponding substituted benzene-1,2-diola or 2-amino-phenol in the presence of 0.2 mg $ZnCl_2$ and KOH (2.5 g), dissolved in 20 mL water. The solution/suspension was refluxed (3 h, 40 °C). Then it was poured on crushed ice and stirred for 2 h. After 24 h at $T = -4$ °C, products obtained, were filtered off, and dried on air.

2.2. Computational methods

Quantum chemical calculations were performed, using GAUSSIAN 09, Dalton2011 and LSDALTON program packages [47–50]. The geometries of the ligands were optimized/re-optimized employing B3LYP method, CAM-B3LYP, and M06-2X functional [51–60]. The force gradient algorithm and standard analytical harmonic vibrational analysis were used. The calculation of the molecular vibrations was achieved, using 6-31+G(d,p) and aug-cc-pVDZ and aug-cc-pVTZ basis sets. The solution propertied were obtained

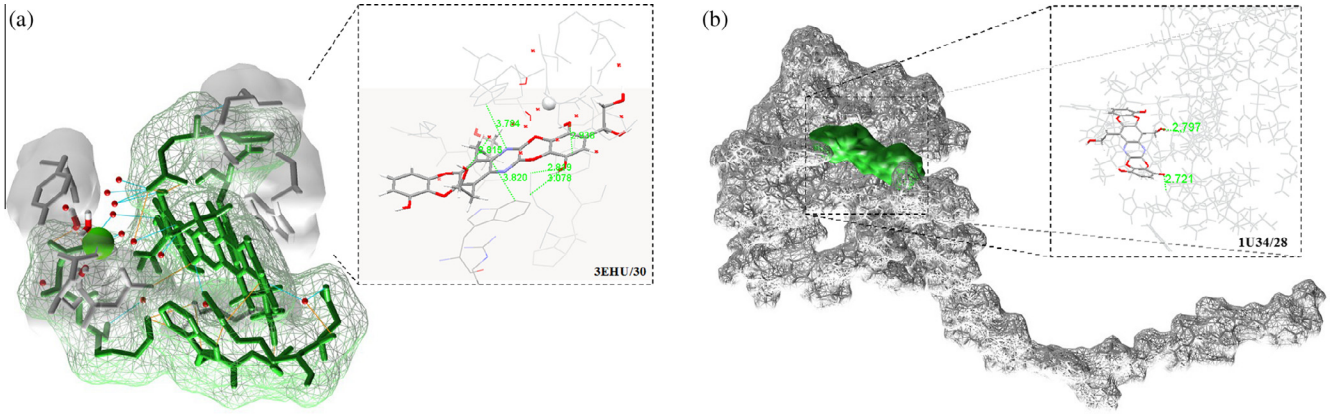

Scheme 1. Optimized drug–receptor interacting systems; Electrostatic surfaces and hydrogen bonding networks.

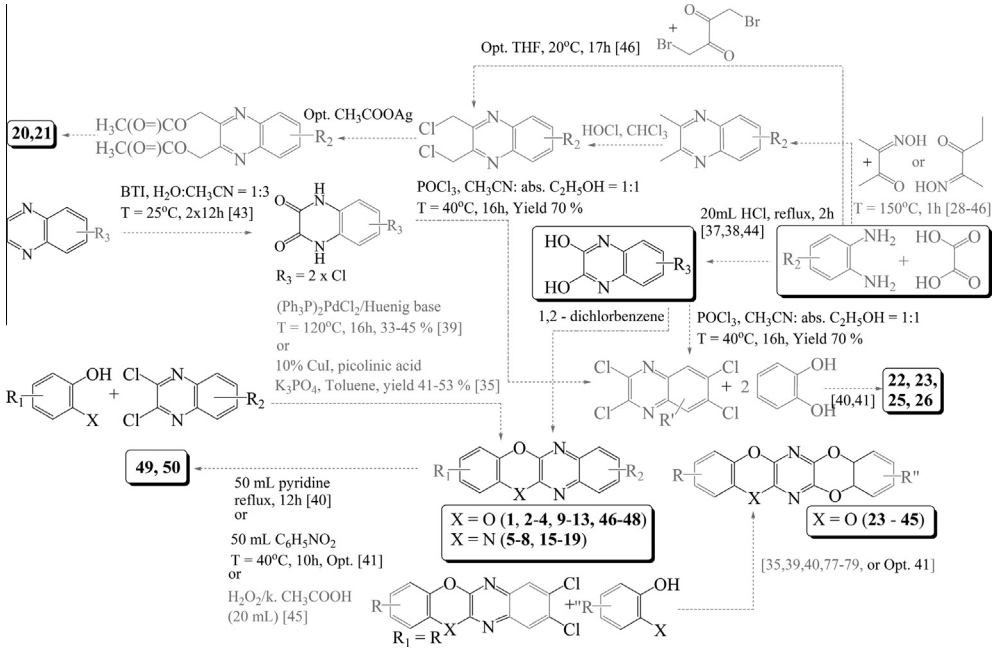

Scheme 2. Synthetic roads for obtaining of substituted quinoxalines.

using TDDFT and PCM (respectively IPCM) approaches [60,61,54]. Both explicit super molecule and micro-hydration approach, includes several $n = 1–3$ water molecules coordinated to a solute. For very large species was used ONIOM method, in which different parts of super molecule was treated at different levels of accuracy, by different basis sets or methods. Molecular mechanics calculations were performed, using DREIDING and UFF [62,63].

The binding affinity of the ligands towards the macromolecular host system can be evaluated, using the theoretical calculations of the "*free energy*", a term which is directly addressed to the geometry and the conformations of the biological systems. A comprehensive presentation of the available quantum mechanical and quantum chemical approaches can be found in [64,65]. To facilitate the interpretation of the theoretical data in our study, allowing to understand the molecular design and the synthetic strategies, a brief description of the theoretical terms are presented herein. The structure of the molecules is determined, using the position of the atoms within the frame of given coordinate systems, nevertheless are they determined experimentally by the single crystal X-ray diffraction or theoretically, using the methods of the quantum chemistry. To a given structure and electronic state, each molecule has a specific energy, which in terms of potential energy of the system, has a value, which can be changed in dependence on the molecular geometry. The equilibrium state of such as system is determined at the minimum of the energy value. Thus, any conformational changes, originating from a concrete drug–receptor interaction mode at molecular engineering level has resulted in a specific free energy profile. In this respect an accurate prediction of the "*free energy*" enables to ensure a meaningful information about the molecular properties. It allows to evaluate, too, is a concrete molecular drug–receptor interacting system is "preferred" one or "not" from a thermodynamic point of view. The thermodynamic most preferred is this system, having the lowest (negative) free energy value. The relationship between "free energy" and "potential energy" has given by Eq. (1).

$$\Delta G = f(PE) \tag{1}$$

The application of Eq. (1) for analytical purposes needs to use a reliable force field and the energy function, which to express maximum representatively the molecular conformation and electronic state of the system to a real structure. Then, in terms of FF calculations, the potential energy of bond bending interaction has given by Eq. (2), where $k_{\theta 2}$ is a bond bending constant, while θ^0 is the equilibrium bond angle. Under a larger deformation it should take into account the anharmonisity, using Eq. (3). The bond stretching energy has given by Eq. (4), where the corresponding k_r and r^0 are bond stretching constant and corresponding interatomic distance at equilibrium. While Eq. (5) gives energy of torsion interaction, where V_i ($i = 1–3$) is torsion force constant, i is periodicity, γ is the phase and ϕ is the torsion angle, respectively. Out-of-plane bending interactions can be given by Eq. (6), where χ is out-of-plane coordinates.

$$E_\theta = k_{\theta 2} \cdot (\theta - \theta^0)^2 \tag{2}$$

$$E_\theta = k_{\theta 2} \cdot (\theta - \theta^0)^2 + \ldots + k_{\theta 6} \cdot (\theta - \theta^0)^6 \tag{3}$$

$$E_r = k_{r2} \cdot (r - r^0)^2 + \ldots + k_{r4} \cdot (r - r^0)^4 \tag{4}$$

$$E_\tau = \sum_\tau V_i \cdot (1 + \cos(i\phi - \gamma)) \tag{5}$$

$$E_\chi = k_\chi \cdot \chi^2 \tag{6}$$

In terms of MM force field Eq. (2) has the form Eq. (7).

$$E_\theta = k_\theta \cdot (1 + \cos\theta) \tag{7}$$

The non-covalent van der Waals and electrostatic interactions can be given by Eqs. (8) and (9).

$$E_{vdW} = \sum_{i<j} \left[\frac{A_{ij}}{R_{ij}^{12}} - \frac{B_{ij}}{R_{ij}^{6}} \right] \tag{8}$$

$$E_e = \frac{q_i q_j}{R_{ij} \cdot \varepsilon} \tag{9}$$

In Eq. (8), A_{ij} and B_{ij} are non-bonded repulsion (Lennard-Jones) and corresponding attraction coefficients, while R_{ij} is the distance between ith and jth atoms. The Eq. (9) has expressed the electrostatic energy as a function of atomic partial charges q_i and q_j, R_{ij} and the dielectric constant (ε), respectively.

In terms of MM force field, the q_i can be given by the function of, δ_{ij} bond increment.

So that, the total energy of a system should express all these energy terms as a sum, which has given by Eq. (10).

$$E = E_r + E_\theta + E_\tau + E_\chi + E_{vdW} + E_e \tag{10}$$

Or Eq. (10) can be written, in a form shown in Eq. (11), where $\Delta G_{\text{non-bond}}$ term means energy of the non-covalent interactions. The relationship between E_i terms in Eq. (10) and ΔG ones has given by Eq. (12), where λ is a parameter involved in the thermodynamic integration approach. It has often been expressed as simple based scalar parameter.

$$\Delta G = \Delta G_r + \Delta G_\theta + \Delta G_\tau + \Delta G_{\text{non-bond.}} + \Delta G_e \tag{11}$$

$$\Delta G = \int \left\langle \frac{dE_r}{d\lambda} + \frac{dE_\theta}{d\lambda} + \frac{dE_\tau}{d\lambda} + \frac{dE_{\text{non-bond.}}}{d\lambda} + \frac{dE_e}{d\lambda} \right\rangle_\lambda d\lambda \tag{12}$$

Given that, in terms of MM calculations the absolute free energy, or Eq. (1), can be expressed by Eq. (13), where E_{MM}, in fact, represents E in Eq. (10). The G_{SF} is solvation free energy, T – temperature and, S_{MM} is the MM entropy. The MM methods uses an improvement of MD for the effective presentation of the energy function. The symbol "G" is used to express the "free energy", while MM energy terms can be found, expressed by symbols "V" or "E" [64,65].

$$G = E_{MM} + G_{SF} - T \cdot S_{MM} \tag{13}$$

The relevant thermodynamic information can be obtained by Eq. (10), using the Monte-Carlo and MD approaches. Our study, involves the second one, which represents an integration of the analytical FF of Newton's Eq. (14). The substitution of Eq. (10) in Eq. (14), accounting for that the force (F) has given by gradient of the FF energy (E') (Eq. (15)), has yielded to a complex partial differential equation, which solution can be obtained, applying a stepwise integration.

$$F = m\frac{\partial^2 x}{\partial x} \tag{14}$$

$$F = -\frac{\partial E(x)}{\partial x} \tag{15}$$

If the free energy is expressed by a classical form from the statistical mechanics point of view (Eq. (16)), where R is gas-constant and T – temperature. The partial function Q has form given by Eq. (17). The C is a constant, x – coordinates and , p – phases, while $H(x,p)$ is the Hamitonian of the system resulting in it energy in terms of atomic coordinates and moments. For a system, having N atoms, V (volume) and T-constants, "G" in Eq. (17) is equal to the "*Helmholtz's free energy*". By contrast, in one isothermal-sobaric system at N,T,P-constants, the "G" is equal to the "*free Gibbs energy*".

$$G = -RT \ln Q \tag{16}$$

$$Q = \iint e^{-\frac{H(x,p)}{RT}} dxdp \tag{17}$$

The substitution of Eq. (17) in Eq. (16) has resulted in Eq. (18), which for two conformations of one system "1" and "2" has the form, shown, using Eq. (19).

$$G = RT \ln \frac{1}{C \iint e^{-\frac{H(x,p)}{RT}} dxdp} \tag{18}$$

$$\Delta G = G_{"2"} - G_{"1"} = -RT \ln \left(\frac{Q_{"2"}}{Q_{"1"}} \right) = -RT \ln \left[\frac{\iint e^{\frac{H_{"2"}(x,p)}{RT}} dxdp}{\iint e^{\frac{H_{"1"}(x,p)}{RT}} dxdp} \right] \tag{19}$$

Given that, if we would like to express the "*binding free energy*" of a drug–receptor system, than $\Delta(\Delta G_{bind})$ gives a difference of two equilibrium states. It gives, too, a difference of the energy of the interacting system (ΔG_{int}), the free energy of the macromolecule in an equilibrium state ($\Delta G_{macromol}$) and the free energy of the isolated drug (or ligand) at the equilibrium state (ΔG_{drug}) as well (Eq. (20)).

$$\Delta(\Delta G_{bind}) = \Delta G_{int} - \Delta G_{macromol} - \Delta G_{drug} = \Delta G_{"2"} - \Delta G_{"1"} \tag{20}$$

A successful theoretical approach, evaluating the energy of solute-solvent interactions is based on PCM. It is applicable to MD, too, in prediction of G_{SF} (Eq. (13)). The method determined the free energy as a sum of the energy of the thermal motion (G_{tm}), cavitation term (G_{cav}), dispersion and repulsion terms (G_{dis} and G_{rep}) and the energy of the electrostatic solute-solvent interactions (G_e), using Eq. (21).

$$G = G_e + G_{rep} + G_{dis} + G_{cav} + G_{tm} \tag{21}$$

A comprehensive description of the theoretical background of this approach and it applicability to various molecular systems can be found [60,61,54,63,64].

Our calculations involve an optimization of the molecular geometry of the isolated ligand molecules, using *ab initio* or DFT methods. By contrast, the geometry of the corresponding macromolecular ensemble was taken from experimental crystallographic or nuclear magnetic resonance 3D structural atomic coordinate datasets, where the application of PCM has resulted to corresponding solvation free Gibbs energy, accounting for calculations at fixed *V*, *P* and, *T*. For the crystallographic input coordinates our calculations involved as well, additional optimization of the molecular geometry allowing to evaluate any possible conformational changes of the macromolecule as a result of solid-state → solution transitions.

The crystallographic and NMR coordinates of the atoms were obtained from Protein Data Bank and were used as input parameters. The pdb-file labelling were used in the discussion section. The initial CRF was 1go9.pdb [1], while for astressin B it was used 2RMD.pdb [6]. The *m*CRFR$_{2\beta}$ first ECD coordinates in complex with astressin B or urocortin were 2JNC.pdb and 2JND.pdb [2,4,10]. Another NMR coordinates for the first ECD of CRFR$_{2\beta}$ was also utilized (1U34.pdb [8]), while for CRFR$_{2\alpha}$ – 3N93.pdb [19]. The computation of CRFR$_1$ was based on 3EHS.pdb and 3EHU.pdb coordinates [3]. Details of full computational procedure can be found in [47–60].

2.3. Statistical methods

The experimental and theoretical spectroscopic data processing was performed, using R4Cal OpenOffice STATISTICs for Windows 7 program packages [66–68]. Baseline corrections, linear and non-linear curve-fitting procedures were applied for interpretation of experimental electronic absorption spectra (Table S1) [69–75]. The statistical significance of each regression coefficient was checked by the use of *t*-test. The model fit was determined by *F*-test. Details can be found in [66–68].

2.4. Physical methods

The UV–VIS and fluorescence spectra ∈ 190–1190 nm using CH_3OH, CH_3CH_2OH, CH_3CN solvents (Uvasol®, Merck) at different concentration range ∈ $1.0.10^{-5}$–$1.0.10^{-6}$ M in 0.921 cm quartz cells were recorded on Tecan Safire Absorbance/Fluorescence XFluor 4 V 4.40 spectrophotometer. The CD spectra were measured on JASCO J-715 polarimeter with 0.5 nm resolution. The solid-state IR-spectra were recorded using KBr-pellets techniques on Thermo-Nicolet 6700 FTIR and Bomem Michelson 100 spectrometer. HPLC2013ESI-MS/MS measurements were performed on TSQ 7000 instrument (Thermo Fisher Inc). Two mobile phase compositions were (A) 0.1% *v*/*v* aqueous HCOOH and (B) 0.1% *v*/*v* HCOOH in CH_3CN. A triple quadrupole mass spectrometer (TSQ 7000 Thermo Electron) equipped with an ESI 2 source was utilized, operating at capillary temperature 180 °C; sheath gas 60 psi, corona 4.5 μA and spray voltage 4.5 kV. Sample was dissolved in CH_3CN (1 mg (mL^{-1})) and was injected in ion source by an auto-sampler (Surveyor) with a flow of pure CH_3CN (0.2 mL min^{-1}). Data were processed by Excalibur 1.4 software. Chromatographic analysis was performed with a Gynkotek (Germering) HPLC instrument, equipped with a preparative Kromasil 100 C18 column (250 × 20 mm, 7 μm; Eka Chemicals) and a UV detector set at 250 nm. The mobile phase was CH_3CN:H_2O (90:10, *v*/*v*) at a flow rate of 4 mL min^{-1}. The HPLC analysis was performed on a Phenomenex (Torrance) RP-18 column (Jupiter 300, 150 × 2 mm, 3 μm). A Shimadzu UFLC XR (Kyoto) instrument, equipped with an auto-sampler, and on-line degasser and column thermostat was also utilized. As stationary phase a Phenomenex Luna Phenyl-Hexyl column (150 × 3 mm i.d., 3 μm particle size) was used. The mobile phase consisted of 0.02% (*v*/*v*) TFA in H_2O (solvent A) and CH_3CN:CH_3OH 75:25 (*v*/*v*; solvent B). Separation was achieved by a gradient analysis starting with 55A-45B, increasing amount of solvent B in 30 min to 75% and 30.1 min to 100% B, stop time 40 min. For equilibration a post time of 15 min was applied. Other parameters: flow rate 0.30 mL min^{-1}, injection volume 5 μL, detection wavelength 280 nm; column temperature 35 °C. Megapore deionized water was used for making aqueous solutions. NMR spectroscopy was performed with a Varian (Palo Alto) Inova 400, a 400 MHz instrument, with anhydrous DMSO-d_6 used as solvent. The NMR spectra were recorded in 1-D and 2-D modes. 2-D NMR techniques included correlation spectroscopy, heteronuclear multibond correlation, and heteronuclear single quantum coherence.

3. Results and discussion

3.1. Macromolecular drugs–receptor interaction and modelling

3D-NMR structure of the apo-form of ECD1-CRF-R$_{2\beta}$ and it complex with astressin (2JND.pdb) have shown [2,4], that the receptor loop involves the following hydrogen bonded amino acid residues $Trp^{109}NH\cdots OHThr^{63}$ (1.6746), $Trp^{71}NH\cdots OCOAsp^{65}$ (1.6051), $Arg^{101}NH\cdots OCOAsp^{65}$ (1.7236) and $Ile^{241}O\cdots NHVal^{113}$ (2.2867 Å). Lowest thermodynamic stability is obtained for the apo- form of ECD1-CRF-R$_{2\beta}$ (2JND), showing ΔE = −405.74 kcal mol^{-1}, (Table 1). The interaction with CRF (2JND/1go9) causes for a decreasing in the thermodynamic stability ($\Delta(\Delta E)$ = |1845.04| kcal mol^{-1}). Lower magnitude order is found for the system 2JND/**Ant** ($\Delta(\Delta E)$ = |46.84| kcal mol^{-1}). ECD1-CRF-R$_{2\beta}$ molecular ensemble can be regarded as less sensible towards an interaction with **Ant.** The

Table 1
Thermodynamics of macromolecular-drug ensembles of $CRFR_1$ and $CRFR_{2\beta}$ receptors; ΔE [kcal mol^{-1}]; The coordinates of the macromolecular receptors are according 3EHS.pdb, 2JND.pdb, 3EHU.pdb and 1U34.pdb.

	1	2	3	4	5	6	7	8	9	10	11	12	13	14	15	16	17	18	19	20
3EHS	−5.034	−36.98	−29.35	−58.48	−65.51	−68.44	−43.36	−49.65	−52.44	−59.54	−58.32	−24.24	−37.36		−53.8	−62.07	−45.96	−58.78	−23.53	−38.98
2JND	−420.3	−445.1	−454.5	−469.5	−476.3	−443.4	−482.2	−480.4	−485.9	−524.2	−481.1	–	−487.9	−469.5	−458.8	−504.0	−494.3	–	−421.6	−453.5
3EHU	−266.3	−303.11	–	−329.9	−327.9	–	−310.4	−327.1	−339.2	−328.7	–	−316.1	−320.1	−316.1	−322.7	−322.1	−314.8	–		−306.2
1U34	4163.8	3387.6	–	4515.5	3484.2	–	4344.2	3405.4	3146.0	3226.4	–	4544.1	2721.3	3420.9	3406.3	3366.9	3329.3	–	3296.3	3978.2
3N96	−12.9	−37.5	−58.3	−45.6	−56.6	–	−41.2	−53.1	−64.1	−64.1	−55.6	−46.2	−53.9	−47.3	−44.4	−49.7	−44.9	–	−6.1	−38.33
	21	22	23	24	25	26	27	28	29	30	31	32	33	34	35	36	37	38	39	40
3EHS	37.38	−17.04	−40.08	−47.76	−46.91	−46.08	−68.57	−72.7	−78.36	−72.12	−79.42	2.29	−9.41	15.89	−32.51	−37.23	−50.46	−51.52	−74.15	−1.34
2JND	−452.7	−458.6	−473.4	−471.9	–	−467.5	−502.5	−495.3	−477.9	−443.3	−474.6	−456.8	–	−447.1	−472.8	−452.1	−470.3	−465.4	−513.6	−433.9
3EHU	−303.9	−281.5	−305.4	−311.1	–	−296.9	−316.4	−329.6	−296.9	−340.5	−343.9	−280.7	−275.1	−270.4	−263.9	−281.0	−292.3	−313.2	−290.6	−256.6
1U34	4576.4	4518.3	4142.9	4380.9	–	3041.5	3906.8	*186.0*	2780.8	3682.0	3517.2	4134.3	4026.9	3491.4	3416.7	4549.0	3320.6	3228.5	2749.4	4559.4
3N96	−27.3	−12.4	−47.3	−46.1	−37.3	–	−58.8	−61.0	−46.7	−28.2	−52.3	−11.4	−15.4	−7.1	−23.8	−21.2	−34.1	−30.5	−40.6	−11.6
	41	42	43	44	45	46	47	48	49	50										
3EHS	−14.68	−21.99	−36.39	−43.93	−47.53	−19.17	−26.07	−38.39	−80.31	−36.09										
2JND	−464.3	−467.8	–	−460.1	−496.9	−491.2	−451.6	–	−456.8	–										
3EHU	−293.8	−260.4	–	−312.8	−327.2	−325.6	−304.7	−314.9	–	–										
1U34	3453.0	3311.6	3484.0	4548.8	3293.8	3266.7	3519.5	4188.9	3402.3	–										
3N96	−14.7	−14.6	–	−29.8	−47.8	−19.8	−22.3	−23.9	–	–										
	Recept.	1go9	2RMD	Ant	Pex	Recept.	1go9	2RMD	Ant											
	Whole macromolecule					*Active loop environment*														
3EHS	−1484.6	−1811.9	−1616.3	−1470.9	−1495.5	10.35	−290.5	−168.1	27.8											
2JND	−405.74	1439.3	−686.93	−358.9	−423.5	–	–	–	–											
3N96	−1497.61	−1835.1	−1798.9	−1457.3	–	5.723	−295.31	−205.83	14.06											
	Recept – active loop environment					Recept. – whole macromol.														
		-sugar	*-sugar-BTB*																	
3EHU	−264.4	−251.28	−201.7	−266.2		−1456.2														
1U34						3488.8														

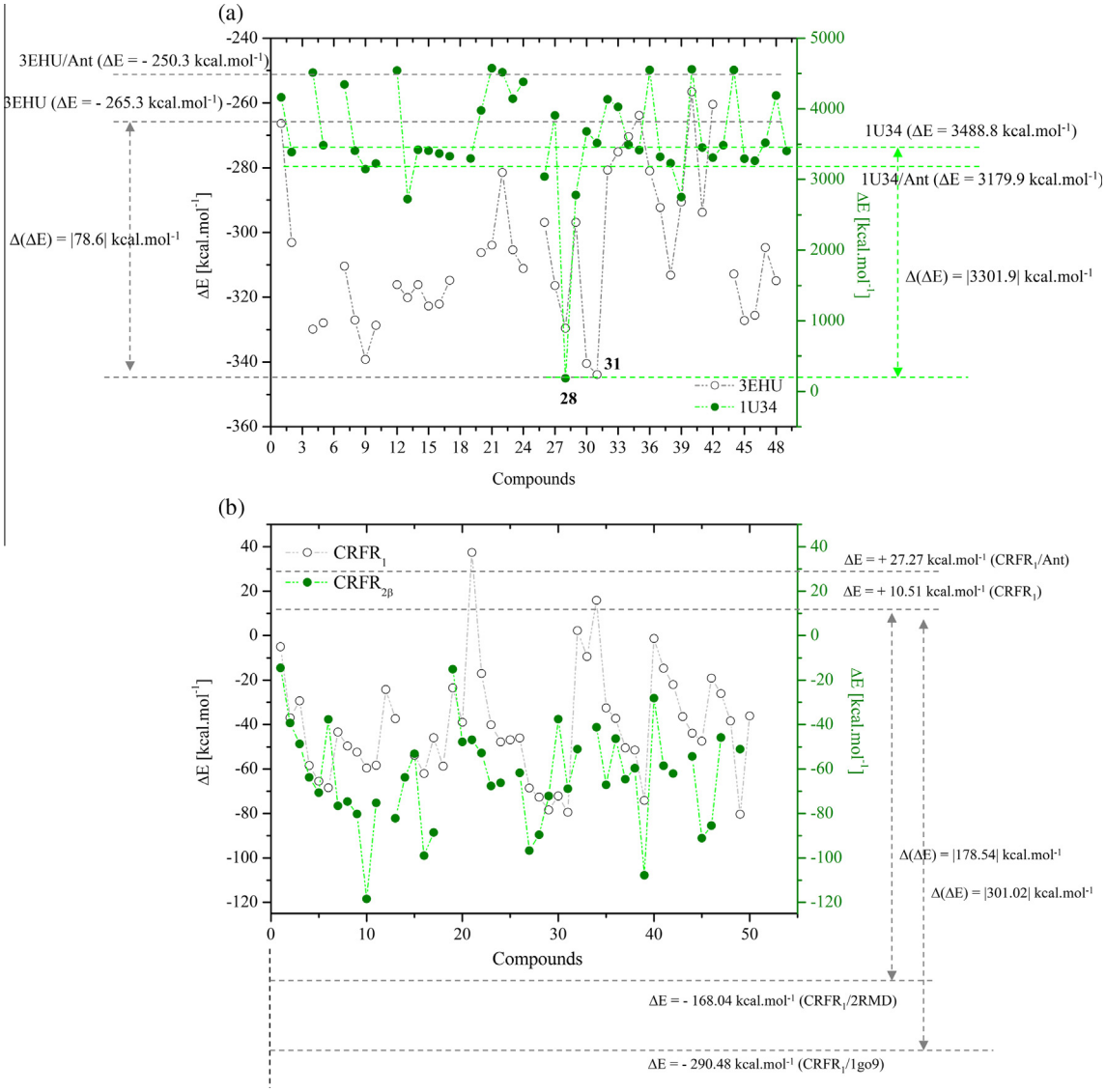

Fig. 1. Thermodynamics of macromolecular-drug ensembles of $CRFR_1$ and $CRFR_{2\beta}$ receptors; The values for the $CRFR_{2\beta}$ receptor systems are corrected with the $\Delta E = -405.74$ kcal mol^{-1}, which is the value of the free of ligand receptor according 3EHS.pdb, 3EHU.pdb, 1U34.pdb 2JND.pdb input coordinates (Non-corrected values are summarized in Table S1).

ΔE values are $\in$ (−405.28) to (−422.05) kcal mol^{-1}), which depends on the corresponding interaction mode **2**–**7** ($\Delta(\Delta E)$ = |16.03| kcal mol^{-1}, Table S3). By contrast, the interaction with astressin B (system 2JND/2RMD) increases the thermodynamic stability ($\Delta(\Delta E)$ = |280.65| kcal mol^{-1}). This tendency, but, having a lower magnitude, is obtained, studying the binding affinity of **Pex** (2JND/**Pex**) ($\Delta(\Delta E)$ = |17.17| kcal mol^{-1}). The interaction of ECD1-CRF-$R_{2\beta}$ with **1**–**50** leads to an increasing in the macromolecular complex stability. The ΔE values are $\in$ (−420.3) to (−513.6) kcal mol^{-1} (Table 1, Fig. 1). Higher affinity is found for the systems, where the interacting ligands are **39**, **16** and **27**. ΔE values of 2JND/**39**, 2JND/**16**, and 2JND/**27** are −513.6, −504.2 and, −502.5 kcal mol^{-1}, respectively. The activity of **39** is 1.21 times higher than this of **Pex**, and 1.33 lower than the corresponding one of astressin B towards interaction with 2JND ECD1-CRF-$R_{2\beta}$. The different binding affinity to the first extracellular domain of CRF-$R_{2\beta}$ is found, using the 3D NMR structures (2JND.pdb [10] and 1U34.pdb [8]). This result may be explained with the change of the macromolecular conformation during the phase transition from the solid-state to solution. The perturbation of the major rearrangement can be explained, too, with the different experimental conditions and factors, mainly involving pH within the frame of values $\in$ 5–7.4. The different protonation type of the macromolecular structure causes for a various intramolecular hydrogen bonding 3D networks, which affect on the free energy of the system (see the theoretical part) and Schemes 1, S2, S4, S9 and, S10, respectively. The interaction with 1go9 or **Ant** results in positive ΔE values (Table S1), meaning a decreasing of the thermodynamic stability of the interacting ensembles. Significant stability is obtained for ligands **2**, **5**, **8**, **11**, **13**, **14**, **19**, **26**, **30**, **34**, **37**–**39**, **41**, **42**, **45**, **46** and **49**, interacting with CRFRs Remarkably stable is complex 1U34/**28** in interaction mode 3, showing a decreasing of $\Delta(\Delta E)$ of |3302.8| kcal mol^{-1}.

To evaluate the possibility for a drugs/CRF interactions, series of different modes (**2**–**11**) are exterminated (Scheme S8, Table S2). The ΔE are $\in$ (−240.6) to (−261.77) kcal mol^{-1}. Of these, all values are higher ones, than the ΔE of 1go9. With these results in mind, we could be assumed that the binding interaction of **Ant** to the macromolecule decreases in the peptidic stability. The active loop of $CRFR_{2\alpha}$ (3N96), involves amino acid Trp^{308}, Arg^{304}, Asp^{305}, Gln^{259}, Trp^{30} and Tyr^{215} residues. Intra-macromolecular target Lys^{255} NH···OAsn^{358} (2.8497 Å) interaction is found. An intra-molecular

hydrogen bonding, which includes the disacchadide ($Tyr^{215}NH\cdots O$ (Sacc) (3.1930 Å)) is also occurred. The $CRFR_{2\alpha}$ apo-form exhibits a comparable macromolecular thermodynamic stability towards the ΔE value of $CRFR_{2\beta}$ (2JND). A $\Delta(\Delta E) = |13.1|$ kcal mol^{-1} is found (Table 1). By contrast, a low affinity of CRF towards $CRFR_{2\beta}$ (2JND) is obtained. The peptide exhibits a significant activity towards $CRFR_{2\alpha}$. The complex is characterized as thermodynamic stable macromolecular ensemble 3N96/1go9, having $\Delta(\Delta E) = |337.49|$ kcal mol^{-1}. The binding affinity of **Ant** to $CRFR_{2\beta}$ is low. An increasing of ΔE value of |40.3| kcal mol^{-1} for the 3N96/Ant complex is obtained. The ΔE of the active loop of 3N96, using the reduced number of atoms, thus localizing only the cavity environment, an approach, which has been discussed in [62], shows ΔE = +5.73 kcal mol^{-1}. The interaction with compounds **1–50** leads to ΔE values $\in$ (−6.5) to (−64.1) kcal mol^{-1}. These results thus highlight to an increasing affinity of the ligands towards $CRFR_{2\alpha}$ (Table 1, Fig. S1). The comparative analysis performed, using the affinity of CRF and astressin B to the CRFRs is based on the following concept: from the ΔE values of 3N96/1go9 and 3N96/2RMD complexes were subtracted the ΔE ones of the systems of interacting peptides themselves. The ΔE values of 1go9 and 2RMD are −267.70 and −165.50 kcal mol^{-1}, respectively. Complexes 3N96/1go9 and 3N96/2RMD, using the reduced number of atoms, which are located around active receptor loop, have ΔE values of −28.01 and −2.6 kcal mol^{-1}, respectively. Derivatives **1–50** exhibit higher affinity towards $CRFR_{2\alpha}$, comparing with the data of 2RMD macromolecule. A higher affinity towards the same receptor subtype, but comparing with CRF (1go9) macromolecule, have the ligands **2**, **17**, **20**, **23–29**, **31**, **37–39**, **44** and **45**, respectively.

The active loop of $CRFR_1$, obtained from 3EHU set of atomic coordinates shows a more complex interacting network, involving Ca^{2+}-ion and solvent water molecules (Scheme 1). The participation of the amino acid residues and solvent molecules: Tyr^{139}, Asp^{335}, Asn^{337}, Trp^{287}, Arg^{283}, Tyr^{194}, Glu^{238}, Gly^{196}, and $H_2O^{654,\ 554,\ 718,\ 535,\ 603,\ 528,\ 641,\ 627,\ 701,\ 657,\ 595,\ 556,\ 708,\ 508\ and\ 505}$, has been observed. The Asp^{308} is involved in $Asp^{308}OCO\cdots Ca^{2+}$ interaction (2.3212 Å) in a monodentate manner. In addition, hydrogen bonds of type $Tyr^{194}OH\cdots OH_2^{528}$ (2.785), $H_2O^{708}\cdots OCOAsp^{308}$ (2.991), $Lys^{334}NH\cdots OH_2^{544}$ (3.322), $H_2O^{506}\cdots O=CAsn^{337}$ (3.251), $H_2O^{556,\ 641}\cdots OCOAsp^{335}$ (3.054, 2.594) and $H_2O^{627}\cdots OH_2^{657}$ (3.377 Å) are found (Schemes S2 and S3). Unlike the $CRFR_{2\alpha}$, the CRF has a lower affinity to $CRFR_1$ macromolecule. A $\Delta(\Delta E)$ value of |13.1| kcal mol^{-1} is found. Similar tendency is obtained, studying the macromolecular complex ensemble 3EHU/2RMD. Like the **Ant** behaviour towards the $CRFR_{2\alpha}$ and $CRFR_{2\beta}$, it interaction to $CRFR_1$ shows ΔE = −266.2 kcal mol^{-1}, assuming an insignificant activity. In spite of various interaction modes studied (Table S1, Schemes S6–S9), the ΔE values $\in$ (−266.2) to (−303.11) kcal mol^{-1} are found. Compounds **1–50** show $\Delta E \in$ (−256.6) to (−343.9) kcal mol^{-1}, when they interact with the macromolecule 3EHU. Highest affinity is obtained for ligands **30**, **31** and **9**, having ΔE values −340.5, −343.9, and −339.2 kcal mol^{-1}, respectively. These values are 1.13–1.11 times higher than the corresponding ΔE one of the system 3HEU/**Ant**. The 3EHU and 3EHS are set of atomic coordinates of $CRFR_1$, and thus ΔE values obtained, agree with the data, which have been reported to [21]. The major rearrangement, *i.e.* the major conformational change of the ECD 3D structure, is obtained as a result of the hormone/macromolecular interactions. The system 3HES is more stable than the corresponding 3HEU one, showing $\Delta E = |28.4|$ kcal mol^{-1}. The interaction with CRF causes for a decreasing of the ΔE of |327.3| kcal mol^{-1}. An increasing of the thermodynamic stability of the complex 3HES/1go9 complex is obtained. The ΔE of 3EHS/1go9 is −290.5 kcal mol^{-1}, accounting for the reduced set of atomic coordinates around the active loop. ΔE of −22.8 kcal mol^{-1} is obtained, evaluating the energy of isolated CRF macromolecule. In this respect, the derivatives **2–20**, **23–31**, **35–39**, **43–45** and **47–50** have higher affinity towards 3HES, than the peptide 1go9. All substances **1–50** show lower ΔE values than this one of the complex 3HES/**Ant**.

3.2. Mass spectrometric methods and synthesis of small molecular ligands

An effective molecular drugs design involves the search of new potent biologically active ligands, having, in addition, possibility to be synthesized under known and well established methodologies, using small number of synthetic stages (or only one single step), causing good-to-excellent yields. With these conditions in mind, the biological *in vitro* and *in vivo* tests are ensured. Furthermore, a chemical substitution within frame of a given molecular template should be taken into account to have, too, a limit of the number of the synthetic stages [17]. In spite of numerous efforts to optimize the synthesis of the non-peptidic CRFRs antagonists such as the derivatives of **Ant** and **Pex** [7], the alkyl-(8-substituted-phenyl-pyrazolo[1,5-a][1,3,5]triazin-4-yl)-amine scaffold has been obtained, using a complex road, involving **6–8** steps, yielding the products $\in$ 76–50%. The feature step has involved a Pd-catalyzing ($PdCl_2/NaHCO_3$) coupling reaction of 6-method-3-bromo-2-methyl pyridine with 4-iodo-4-methylisoxazole. Next isomerization under basic experimental conditions ($NaOCH_3/CH_3OH$) has yielded to β-ketonitrile as sodium enolate form [7]. The optimization of the reaction scheme has resulted in isolation of core of hydroxypyrazolotriazine moiety, using consecutive cyclizations under milder reaction conditions. The chloropyrazolotriazine intermediate has been achieved, using catalytic $POCl_3$/DABCO process, which has resulted in ligands, having purity higher than 99.5%, but an overall yield of 68% within the frame of a six steps synthesis has been reported [7]. The recently reported 2,N,N-trialkil-5-alkilsulfanyl-N′-phenyl-pyrimidine-4,6-diamine type agonists have been obtained in excellent yields, but also the synthetic scheme has involved five steps, using $POCl_3$ and $Pd_2(dba)_3$ catalysts [18].

In parallel, the significant advantages of the molecular models **1–50** as potential candidates, having application for imaging and brain diagnostic are no dough their optical EAs and Fs properties. But they can be obtained using the facile synthetic scheme, having limited number of steps (one-step-synthesis), showing good-to-excellent yields (Scheme 2) as well. The synthesis of derivatives containing [1,4]dioxino[2,3-b]pyrazine motif has already been described [28–46]. But, due to a low solubility of non-substituted analogous (X = N, or O, Scheme 2) structural studies and elucidation of their optical properties have scarce been reported [35,76–78]. Decades achievements in the optimization of synthetic roads have resulted in mostly unsatisfactory yields and competitive formation of various unwanted products of interaction, showing, in parallel, difficult experimental procedures, expensive and detrimental organometallic and/or inorganic precursors. Among the various strategies tested in our study, we have chosen to present only those ones yielding to small number of unwanted competitive products. Thus, the interaction of non-substituted 2,3,6,7-tetrachloro-quinoxaline and it 5,8-disubstituted derivatives with benzene-1,2-diol, using the synthetic approach, which has been reported in [40,41] yielded to **22**, **23**, **25** and **26**. By contrast, the asymmetric substituted derivatives **28–45** were unable to obtain, employing the shown direct condensation of the reagents (Fig. 2). Interaction of (2,3,6,7-tetrachloro-8-hydroxymethyl-quinoxalin-5-yl)-methanol with benzene-1,2-diol results to 96% yield of the product **24**. While, the effort to obtain compound **32** under the same experimental conditions, involving benzene-1,2-diol, 2,3,6,7-tetrachloro-quinoxaline and benzo[1,3]dioxole-5,6-diol results to isolation of **22** and, in parallel, an unwanted disubstituted benzo[1,3]dioxole analogue.

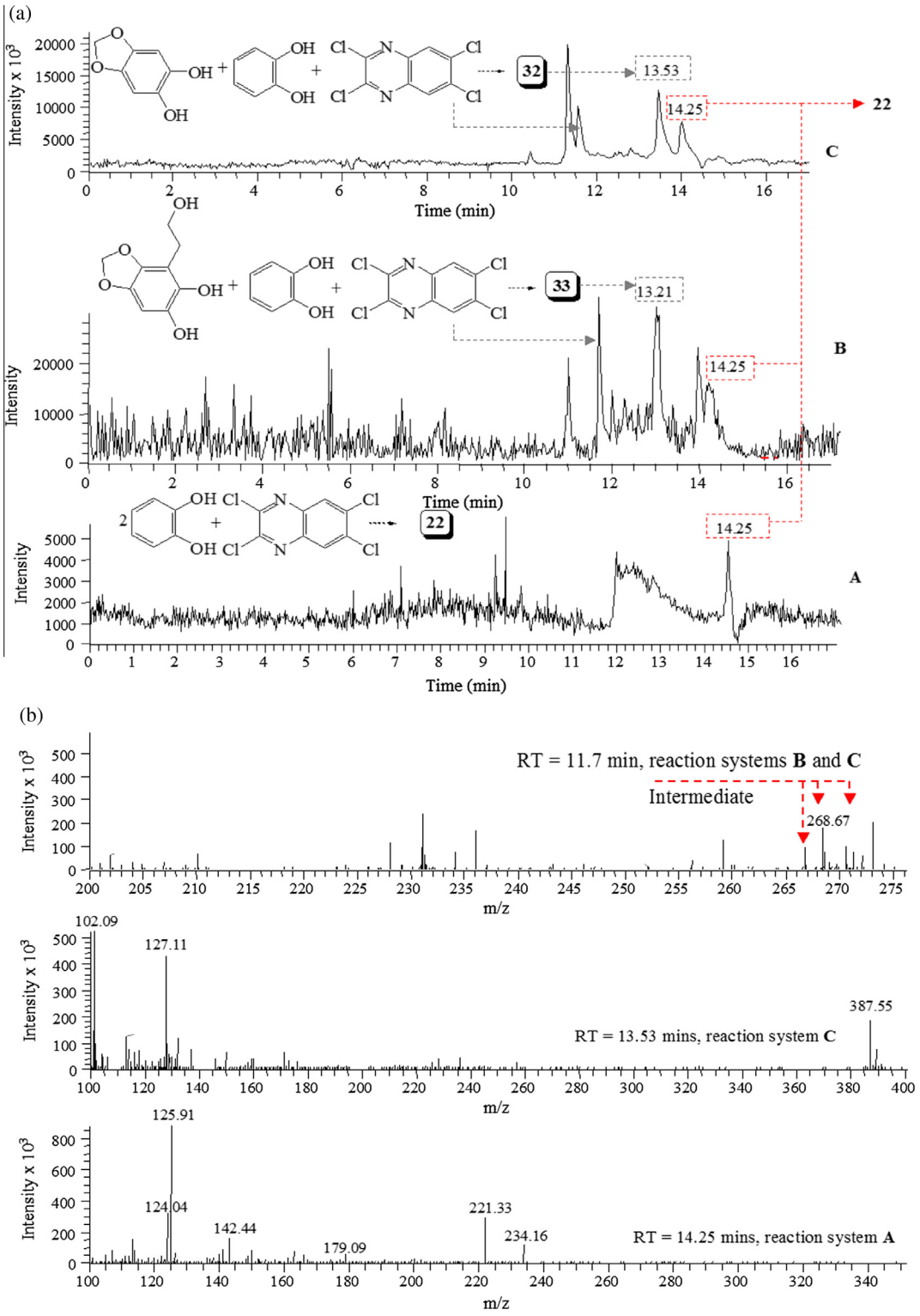

Fig. 2. Chromatogram; Chemical diagram of reacting chemicals and products **22**, **32**, **33**, respectively; ESI-MS spectrometric data.

3.3. Optical spectroscopic properties of the small molecular ligands

The theoretical modelling and design for the derivatives **1–50**, involves a prediction and experimental elucidation of their EAs and Fs properties. The results are listed in Tables S1 and 2. The electronic transitions are n → π* and π → π* types, having relative Fs and Ps quantum yields ($S_1(n,\pi^*) \rightarrow S_0$ and $T_1(\pi,\pi^*) \rightarrow S_0$) depending on the laser excitation energy as well as environmental factors such as T, P or condense phase intra/intermolecular interactions [35,76–78]. The change of $S_0 \rightarrow S_1$ excitation to $S_0 \rightarrow S_2$ assumes a slow redistribution of the vibrational energy between $S_1(n,\pi^*)$ and $S_2(\pi,\pi^*)$ levels through inter-system crossing of the optical population. For an isolated quinoxaline molecular skeleton such as for example, compounds **20** and **21** (Scheme S1) it has been shown $\lambda^{abs} = 315$, $\lambda^{Fs} = 809$ and $\lambda^{Ps} = 629$ nm in C_2H_5OH at 293 and 77 K ($\lambda_{ex} = 365$ nm) [35,76]. The replacement of an oxygen

Table 2
Experimental EAS and Fs spectra [λ_{ex}, nm] (ε_ν, [l mol^{-1} cm^{-1}]).

1									2								
CH_3CH_2OH			C_6H_{12}		CH_3CN		CH_3COOH		CH_3CH_2OH			C_6H_{12}		CH_3CN		CH_3COOH	
λ^{abs}	ε_ν	Fs	λ^{abs}	ε_ν	λ^{abs}	ε_ν	λ^{abs}	ε_ν	λ^{abs}	ε_ν	Fs	λ^{abs}	ε_ν	λ^{abs}	ε_ν	λ^{abs}	ε_ν
–	–	552.1	–	–	–	–	–	–	–	–	590.4	–	–	–	–	–	–
–	–	440.8	–	–	–	–	–	–	–	–	576.3	–	–	–	–	–	–
–	–	409.2	–	–	–	–	–	–	–	–	510.0	–	–	–	–	–	–
420.12	5871	–	400.3	4481	417.3	6509	434.8	3890	443.8	6910	–	456.2	6540	432.5	3561	414.5	1232
410.21	8532	–	397.1	3107	410.4	7990	427.1	7531	427.3	5771	–	450.2	5809	410.1	4679	409.2	2418
397.62	3907	–	369.2	2961	399.5	4210	401.2	4889	410.6	5318	–	431.2	2451	398.7	1782	366.5	1109
3									9								
–	–	599.2	–	–	–	–	–	–	–	–	623.8	–	–	–	–	–	–
–	–	570.2	–	–	–	–	–	–	–	–	598.3	–	–	–	–	–	–
–	–	519.3	–	–	–	–	–	–	–	–	550.7	–	–	–	–	–	–
442.2	6702	–	452.1	7432	433.2	3566	415.2	1145	462.3	7890	–	460.9	6543	469.2	2245	470.8	3465
425.1	5544	–	451.7	3251	418.6	4690	410.4	2455	444.3	9412	–	467.5	7901	470.5	3761	460.5	4460
419.2	1356	–	433.2	2444	399.5	1770	369.6	1217	405.8	3345	–	439.1	4052	440.3	2775	413.8	3220
10									15								
–	–	580.4	–	–	–	–	–	–	–	–	593.2	–	–	–	–	–	–
–	–	562.6	–	–	–	–	–	–	–	–	572.8	–	–	–	–	–	–
–	–	530.2	–	–	–	–	–	–	–	–	555.1	–	–	–	–	–	–
470.1	8790	–	468.3	5782	460.1	2132	473.1	3580	480.5	9642	–	470.5	3571	462.5	4670	480.5	4328
461.8	9554	–	463.1	6834	457.2	3446	470.3	4056	468.3	7654	–	458.3	8872	466.9	2189	469.0	5189
440.2	7345	–	440.5	5312	445.2	2290	438.4	2301	445.0	1701	–	432.8	2290	440.3	1098	453.8	2208
20									21								
–	–	343.7	203.8	17,893	–	–	–	–	–	–	346.9	202.5	15,681	–	–	–	–
–	–	306.2	215.2	13,342	–	–	–	–	–	–	307.1	222.8	14,901	–	–	–	–
233.8	22,874	277.8	235.8	10,907	235.1	22,800	–	–	237.9	18,221	259.4	240.6	11,667	236.3	21,320	–	–
310.6	9332	–	307.6	6508	317.7	6500	312.8	6540	315.1	10,304	–	310.2	8379	320.8	7400	310.3	48,210
320.7	4208	–	–	–	–	–	–	–	327.6	5501	–	–	–	342.6	915	332.8	3703
349.2	700	–	–	–	–	–	354.7	800	350.8	1056	–	–	–	–	–	355.1	1055
27									29								
–	–	588.1	–	–	–	–	–	–	–	–	645.7	–	–	–	–	–	–
–	–	569.2	–	–	–	–	–	–	–	–	596.2	–	–	–	–	–	–
–	–	544.0	–	–	–	–	–	–	–	–	563.8	–	–	–	–	–	–
482.4	7890	–	459.3	3261	466.0	2131	485.7	3780	493.8	9567	–	496.3	4681	483.9	3301	480.4	3432
470.2	10,011	–	468.0	7956	451.1	3415	464.5	4915	481.5	10,057	–	479.0	7932	463.8	8764	494.1	5018
452.1	5790	–	445.1	5417	448.6	1906	445.6	3344	460.0	4381	–	467.2	5819	403.3	3022	414.1	1308
42																	
–	–	597.3	–	–	–	–	–	–									
–	–	588.2	–	–	–	–	–	–									
–	–	540.0	–	–	–	–	–	–									
489.3	9654	–	498.2	6790	469.3	5890	480.0	5617									
477.2	10,014	–	477.0	7904	470.3	6914	478.2	6088									
450.6	8673	–	444.1	4417	462.8	3367	440.2	4670									

atom in molecular scaffold benzo[5,4][1,4]dioxino[2,3-b]quinoxaline (structure of type **3**) with nitrogen in 12H-5-oxa-6,11,12-triaza-naphthacene (structure of type **5**) results in a hypsochromic effect of EAS and Fs sub-component maxima ∈ 14–55 nm (Table 2, S1). Full replacement of the O-centres with nitrogen ones in 5,12-dihydro-quinoxalino[2,3-b]quinoxaline causes to intensive EAs sub-maximum at 415 nm (ε_ν = 23,789 l mol^{-1} cm^{-1}, CH_3OH). The Fs spectra are characterized as series of maxima ∈ 450–650 nm (λ, nm; E, eV; f; 638.3 (E = 1.9426, f = 0.0000), 530.5 (E = 2.3369, f = 0.0000), 497.5 (E = 2.4921, f = 0.2234), 303.2 (E = 4.0886, f = 0.0071), and 282.6 (E = 4.3867, f = 0.0000)). Substituents of 2-hydroxymethyl-malonamic acid type in **12** and conjugated almost planar molecular architecture in **24** lead to a batochromic shifting of CT-band of Δν ∈ 59–44 nm, comparing with the optical properties of molecular template **1**.

3.4. Nuclear magnetic resonance data

In spite of known synthetic reports on quinoxalines, the methodological nuclear magnetic resonance examinations have scarce been represented. The data encompass only simply substituted quinoxaline skeleton in derivatives **20, 21,** having-Cl, $-OCH_3$ or $-CH_3$ substituents at C^{13}, C^{14}, C^2 and/or C^3 positions of the isolated condense molecular ring system (Scheme S1) [76–78]. The non-substituted derivatives show ^{13}C NMR [77)] (J) coupling C(13,14) constants $^1J_{CH}$ = 181.9, $^2J_{CH}$ = 11.4; C(1,4) $^1J_{CH}$ = 162.6, $^3J_{CH}$ = 6.5; and C(2,3), $^1J_{CH}$ = 159.4, $^3J_{CH}$ = 9.1 Hz, respectively. The ^{13}C NMR signals of C^1, C^2, C^3, C^4, C^{13} and C^{14} are ∈ 128.3–130.9, 128.3–127.8, 128.9–130.8, 127.9–129.0, 144.4 and 143.6 ppm, respectively. The isolated derivatives **1**–**3**, **9**, **10**, **15**, **27**, **29** and **42**, have the corresponding signals ∈ 128.3–130.9 ppm. The replacement of the C**H-**centre with C**O**(R) substituent causes for a shifting of carbon (C2,3) signals towards the low-fields Δδ = 13 ppm. The C^1**H**–C^4**H** proton signals of non-substituted quinoxaline have been observed as multiplet ∈ 7.49–7.59 ppm [77]. The reported herein derivatives exhibit ^{1}H NMR peaks of C^1**H**–C^4**H** ∈ 7.9–7.16 ppm. The coupling constants are J = 3.4 and 7.6 Hz, respectively.

4. Conclusion and outlook

The study, first in the literature, has outlined a new synthetic chemical class of substances, based on the quinoxaline molecular

scaffold as potent ligands towards the corticotropin-releasing factor receptor types 1 and 2. Despite numerous research efforts which have been devoted to molecular design of selective ligands to CRFRs, the largest part of the models and experimental design carried out have involved the derivatives of phenyl-7H-pyrrolo[2,3-d]pyrimidin-4-yl)-amine, phenyl-pyrazolo[1,5-a][1,3,5]triazin-4-yl)-amine or 2,N,N-trialkil-5-alkilsulfanyl-N′-phenyl-pyrimidine-4,6-diamine or peptidic ligands analogous of astressin B. Having acquired our theoretical information presented here about the binding affinity of series of fifty model molecules based on the quinoxaline molecular skeleton towards the $CRFR_1$, $CRFR_{2\alpha}$ and $CRF_{2\beta}$ macromolecules as well as their theoretical and experimental optical properties, the following conclusions might be drawn:

(i) The substitution in the quinoxaline molecular scaffold allows to obtain highly selective ligands towards different $CRFR_1$, $CRFR_{2\alpha}$ and $CRF_{2\beta}$ receptor subtypes.
(ii) The synthetic efforts of the selected most prominent ligands have shown that these derivatives can be obtained within the frame of one-step synthetic pathways under mild experimental conditions, using Fischer and Hinsberg methods, resulting in good-to-excellent yields.
(iii) The ligands have easy tunable fluorescence properties $\in$ 500–700 nm, and strongly characteristic spectroscopic profile, allowing it qualitative and quantitative determination.

Given that, the quinoxaline molecular template appears prominent scaffold for design and synthesis of selective CRFRs ligands for fluorescence imaging, monitoring and brain diagnostics.

Acknowledgments

The authors thank Deutscher Akademischer Austausch Dienst, Deutsche Forschungsgemeinschaft, Central intrumental laboratories for structural analysis at Dortmund University of Technology (Germany) and analytical and computational laboratories at Institute of Environmental Research at the same University. Conflict of interests: Michael Spiteller has received research grant (Deutsche Forschungsgemeinschaft 255/22-1); Bojidarka Ivanova has received research grant (Deutsche Forschungsgemeinschaft, 255/22-1).

Appendix A. Supplementary material

Chemical diagram (Scheme S1); Thermodynamics of drugs–receptor interactions of **1**–**50**, CRF, **Ant**, and astressin B with $CRFR_{2\alpha}$, $CRFR_{2\beta}$, and $CRFR_1$ (Tables S1, S2; Fig. S1; Schemes S2–S10); EAs and Fs of **1**–**50** (Table S3); Experimental (analytical data). Supplementary data associated with this article can be found, in the online version, at http://dx.doi.org/10.1016/j.bioorg.2014.10.008.

References

[1] J. Broadbear, G. Winger, J. Rivier, K. Rice, J. Woods, Neuropsychopharmacology 29 (2004) 1112–1121.
[2] A. Pioszak, N. Parker, K. Suino-Powell, H. Xu, J. Biol. Chem. 283 (2008) 32900–32912.
[3] R. Briscoe, C. Cabrera, T. Baird, K. Rice, J. Woodsa, Brain Res. 881 (2000) 204–207.
[4] C. Grace, M. Perrin, J. Gulyas, M. DiGruccio, J. Cantle, J. Rivier, W. Vale, R. Riek, PNAS 104 (2007) 4858–4863.
[5] G. Spyroulias, S. Papazacharias, G. Pairas, P. Cordopatis, Eur. J. Biochem. 269 (2002) 6009–6019.
[6] C. Grace, M. Perrin, J. Cantle, W. Vale, J. Rivier, R. Riek, J. Am. Chem. Soc. 129 (2007) 16102–16114.
[7] S. Broxer, M. Fitzgerald, C. Sfouggatakis, J. Defreese, E. Barlow, G. Powers, M. Peddicord, B. Su, Y. Tai-Yuen, C. Pathirana, J. Sherbine, Org. Process Res. Dev. 15 (2011) 343–352.
[8] C. Grace, M. Perrin, M. DiGruccio, C. Miller, J. Rivier, W. Vale, R. Riek, PNAS 101 (2004) 12836–12841.
[9] S. Whitea, R. Acierno, K. Ruggiero, K. Koenen, D. Kilpatrick, S. Galea, J. Gelernter, V. Williamson, O. McMichael, V. Vladimirov, A. Amstadter, J. Anxiety Disorders 27 (2013) 678–683.
[10] C. Grace, M. Perrin, J. Gulyas, M. DiGruccio, J. Cantle, J. Rivier, W. Vale, Roland Riek, PNAS 104 (2007) 4858–4863.
[11] R. Manuel, J. Metz, G. Flik, W. Vale, M. Huising, Gen. Compar. Endocrinol. 202 (2014) 69–75.
[12] B. Reyes, D. Bangasser, R. Valentino, E. Van Bockstaele, Life Sci. 112 (2014) 2–9.
[13] T. Retson, B. Reyes, E. Van Bockstaele, Progr. Neuro-Psychopharmacol. Biol. Psychiatry 56 (2015) 66–74.
[14] S. Fox, J. Roman, G. Cizza, T. Veenstra, H. Issaq, J. Sep. Sci. 28 (2005) 332–336.
[15] L. Hsin, E. Webster, G. Chrousos, P. Gold, W. Eckelman, C. Contoreggi, K. Rice, J. Label. Comp. Radiopharmaceut. 43 (2000) 899–908.
[16] P. Gilligan, T. Clarke, L. He, S. Lelas, Y. Li, K. Heman, L. Fitzgerald, K. Miller, G. Zhang, A. Marshall, C. Krause, J. McElroy, K. Ward, K. Zeller, H. Wong, S. Bai, J. Saye, S. Grossman, R. Zaczek, S. Arneric, P. Hartig, D. Robertson, G. Trainor, J. Med. Chem. 52 (2009) 3084–3092.
[17] M. Masood, E. Farrant, I. Morao, M. Bazin, M. Perez, M. Bunnage, S. Fancy, T. Peakman, Bioorg. Med. Chem. Lett. 22 (2012) 723–728.
[18] B. Kuppast, K. Spyridaki, G. Liapakis, H. Fahmy, Eur. J. Med. Chem. 78 (2014) 1–9.
[19] K. Pal, K. Swaminathan, H. Xu, A. Pioszak, J. Biol. Chem. 285 (2010) 40351–40361.
[20] K. Hollenstein, J. Kean, A. Bortolato, R. Cheng, A. Dore, A. Jazayeri, R. Cooke, M. Weir, F. Marshall, Nature 499 (2013) 438–445.
[21] K. Pal, K. Melcher, H. Xu, Acta Pharmacol Sin. 33 (2012) 300–311.
[22] K. Spyridaki, M. Matsoukas, A. Cordomi, K. Gkountelias, M. Papadokostaki, T. Mavromoustakos, D. Logothetis, A. Margioris, L. Pardo, G. Liapakis, J. Biol. Chem. 289 (2014) 18966–18977.
[23] A. Thompson, M. Verheij, J. van Muijlwijk-Koezen, S. Lummis, R. Leurs, I. de Esch, ChemMedChem 8 (2013) 946–955.
[24] M. Gogora-Benitez, J. Tulla-Puche, F. Albericio, Chem. Rev. 114 (2014) 901–926.
[25] S. Kouam, A. Ngouonpe, A. Bullach, M. Lamshoft, G. Kuigoua, M. Spiteller, Fitoterapia 91 (2013) 199–204.
[26] F. Talontsi, M. Lamshoft, J. Bauer, A. Razakarivony, B. Andriamihaja, C. Strohmann, M. Spiteller, J. Nat. Prod. 76 (2013) 97–102.
[27] S. Kusari, S. Tatsimo, S. Zuehlke, F. Talontsi, S. Kouam, M. Spiteller, Angew. Chem. Int. Ed. 53 (2014) 1–5.
[28] (a) J. Pressler, R. Beckert, S. Raud, R. Menzel, E. Birckner, W. Guenther, H. Goerlsc, Verlag Zeitschrift Naturforschung (2012) 367–371.
[29] H. Woodburn, E. Hoffman, J. Organic. Chem. 23 (1957) 261–268.
[30] D. Villemin, B. Martin, Int. J. Rapid Commun. Synth. Org. Chem. 25 (1995) 2319–2326.
[31] N. Agarwal, A. Sharm, R. Jamwal, C. Atal, T. Torres, Liebigs Ann. Chem. (1987) 921–925.
[32] I. Abramov, A. Smirnov, S. Ivanovskii, M. Abramova, V. Plakhtinskii, M. Belysheva, Mendeleev Commun. 11 (2001) 80–81.
[33] A. Elwahy, Tetrahedron 56 (2000) 897–907.
[34] R. Kuhn, P. Skrabal, P. Fischw, Tetrahedron 24 (1968) 1843–1848.
[35] M. Schaffroth, B. Lindner, V. Vasilenko, F. Rominger, U. Bunz, J. Org. Chem. 78 (2013) 3142–3150.
[36] M. El-Haj, B. Dominy, J. Johnston, M. Haddadiann, C. Issidorides, J. Org. Chem. 37 (1978) 589–593.
[37] O. Hinsberg, J. Liebigs Ann. Chem. 319 (1901) 257–286.
[38] O. Fischer, E. Hepp, Ber. Dtsch. Chem. Ges 23 (1890) 2789–2793.
[39] O. Tverskoy, F. Rominger, A. Peters, H. Himmel, U. Bunz, Angew. Chem. 123 (2011) 3619–3622.
[40] R. Wolf, C. Marvel, J. Polymer Sci. A-1 7 (1969) 2481–2491.
[41] F. Kehrmann, C. Bener, Helv. Chim. Acta 8 (1925) 16–20.
[42] J. Hartwig, Accts Chem. Res. 41 (2008) 1534–1544.
[43] L. Troian-Gautier, J. De Winter, P. Gerbaux, C. Moucheron, J. Org. Chem. 78 (2013) 11096–11101.
[44] Z. Kazimierczuk, W. Pfleiderer, Liebigs Ann. Chem. (1982) 754–761.
[45] M. Greer, J. Duncan, J.D. Blackstock, Tetrahedron Lett. 38 (1997) 7665–7668.
[46] Q. Liu, Z. Yao, X. Zhao, Z. Zhao, X. Wang, Organometallics 32 (2013) 3493–3501.
[47] M. Frisch et al., Gaussian 09, Gaussian Inc., Pittsburgh, PA, 2009.
[48] GausView03; <http://www.gaussian.com/g_prod/gv3.htm>.
[49] DALTON, a molecular electronic structure program, Release Dalton2011, 2011. see <http://daltonprogram.org>.
[50] LSDALTON, a linear scaling molecular electronic structure program, Release Dalton2011, 2011. <http://daltonprogram.org/>.
[51] D. Crawford, Theor. Chem. Acc. 115 (2006) 227–245.
[52] F. De Proft, P. Geerlings, Chem. Rev. 101 (2001) 1451–1464.
[53] B. Ivanova, M. Spiteller, Biopolymers 93 (2010) 727–734.
[54] B. Mennucci, J. Tomasi, R. Cammi, J. Cheeseman, M. Frisch, F. Devlin, S. Gabriel, P. Stephens, J. Phys. Chem. A 106 (2002) 6102–6113.
[55] Y. Zhao, D. Truhlar, Accts. Chem. Res. 41 (2008) 157–167.
[56] Y. Zhao, D. Truhlar, Theor. Chem. Acc. 120 (2008) 215–241.
[57] V. Hehre, L. Radom, P. Schleyer, J. Pople, Ab Initio Molecular Orbital Theory, Wiley, New York, 1986.
[58] D. Woon, T. Dunning, J. Chem. Phys. 98 (1993) 1358–1371.
[59] E. Meyer, R. Castellano, F. Diederich, Angew. Chem. Int. Ed. 42 (2003) 1210–1250.

[60] J. Tomasi, B. Mennucci, R. Cammi, Chem. Rev. 105 (2005) 2999–3093.
[61] M. Cossi, N. Rega, G. Scalmani, V. Barone, J. Comput. Chem 24 (2003) 669–681.
[62] B. Ivanova, M. Spiteller, Int. J. Biol. Macromol. 65 (2014) 314–324.
[63] B. Ivanova, M. Spiteller, Biopolymers 97 (2012) 134–144.
[64] P. Schreiner, W. Allen, M. Orozco, W. Thiel, P. Willett, Computational Molecular Science, Wiley, West Sussex, Berlin, 2014. vols. 1 (pp. 1–507), 2 (pp. 513–1256); 3 (pp. 1263–1625) and 5 (pp. 2531–2843).
[65] P.vR. Schleyer, N. Allinger, T. Clark, P. Kollman, H. Schaefer III, Encyclopedia of Computational Chemistry, vol. 2, Wiley, West Sussex, 1998. pp. 813–1517.
[66] http://de.openoffice.org/.
[67] C. Kelley, Iterative Methods for Optimization, SIAM Frontiers in Applied Mathematics, vol. 18, 1999.
[68] K. Madsen, H. Nielsen, O. Tingleff, Informatics and Mathematical Modelling, second ed., DTU Press, 2004.
[69] R. Stoesser, M. Siegmund, G. Westphal, Tetrahedron 34 (1978) 2701–2704.
[70] S. Yamauchi, M. Terazima, N. Hirota, J. Phys. Chem. 89 (1985) 4804–4808.
[71] C. Lin, W. Hsu, C. Yang, M. El-Sayed, J. Phys. Chem. 91 (1987) 4556–4559.
[72] R. Podsiad1y, K. Podemska, A. Szymczak, Dyes Pigm. 91 (2011) 422–426.
[73] J. Narewska, R. Strzelczyk, R. Podsiadly, J. Photochem. Photobiol. A 212 (2010) 68–74.
[74] T. Itoh, Spectrochim. Acta A 59 (2003) 3019–3027.
[75] B. Lindner, J. Engelhart, M. Mrken, O. Tverskoy, A. Appleton, F. Rominger, K. Hardcastle, M. Enders, U. Bunz, Chem. Eur. J. 18 (2012) 4627–4633.
[76] H. McNab, J.C.S. Perkin I (1982) 357–363.
[77] S. Paul, B. Basu, Tetrahedron Lett. 52 (2011) 6597–6602.
[78] G. Vermeersch, J. Marko, N. Febvay-Garot, S. Caplain, A. Lablache-Combier, J. Chem. Soc. Perkin Trans. II (1984) 43–47.